IEEE Access
Multidisciplinary | Rapid Review | Open Access Journal

Received September 21, 2018, accepted October 8, 2018, date of publication October 17, 2018, date of current version November 9, 2018.

Digital Object Identifier 10.1109/ACCESS.2018.2876011

High Power, Thermally Efficient, X-band 3D T/R Module With Calibration Capability for Space Radar

ANTONIO FINA[1], ALESSANDRO DI CARLOFELICE[2], AND FRANCESCO DE PAULIS[2], (Member, IEEE)

[1]Thales Alenia Space, 67100 L'Aquila, Italy
[2]Department of Industrial and Information Engineering and Economics, University of L'Aquila, 67100 L'Aquila, Italy

Corresponding author: Antonio Fina (antonio.fina@thalesaleniaspace.com)

This work was supported by the Italian Ministry of Economic Development (MISE: Ministero dello Sviluppo Economico) in the frame of the **L**'**A**quila **SP**ace **EX**cellence (LASPEX) R&D Project.

ABSTRACT Earth observation from space radar is based on the active electronically steerable antenna (AESA) whose performances count on reliable and powerful transmit/receive modules (TRM). To this aim, as a follow-up of the successful demonstration of a low-footprint transmit/receive hybrid module concept based on 3-D packaging and interconnect technologies (3DTRM), the interest for carrying out additional development work took a further step aiming at achieving a three-fold module performance improvement as well as at consolidating the novel proposed 3-D technology for space applications. First, the possibility of performing an AESA highly accurate calibration was implemented by embedding a wide band, high directivity directional coupler in the module circuitry without any total module footprint increase. Second, the heat extraction capability of the metal-ceramic hermetic package was enhanced through a re-design of the monolithic microwave integrated circuit (MMIC)-to-sink interface. And finally, the gallium arsenide (GaAs) MMIC high power amplifier (HPA) of the first 3DTRM version was replaced by a gallium nitride (GaN) HPA MMIC, obtaining both a higher transmit output power at 5 dB of compressed gain and an improved power added efficiency (PAE) at module level.

INDEX TERMS 3D multichip module (MCM) technology, 3D packaging, AESA, low temperature co-fired ceramics (LTCC), transmit/receive (T/R) module, GaN, PAE, directional coupler.

I. INTRODUCTION

The recent progresses in the earth observation systems are driven by the development of a variety of applications emerging in everyone daily life as well as involving many scientific research fields [1], [2]. The huge amount of data collected by instruments on board of orbiting satellites represents the key requirement for developing accurate weather forecast, for monitoring the earth surface (i.e. thickness of the polar ice, the water and air pollution etc. . .), for agricultural purposes among many other applications [3]–[6]. The ever-growing requirements given in terms of image resolution, feature discrimination, penetration depth beyond ground and water surfaces calls for more powerful observation instruments. These application constrains translate into Synthetic Aperture Radar (SAR) systems and the related Active Electronic Steerable Antennas (AESA) being characterized by larger transmitting power, broader operational bandwidth, higher sensitivity, wider steering capability etc. . . [7]–[9]. The key element in this type of space antennas is the transmit/receive module (TRM) [10]–[13].

To this aim, a preliminary novel 3D packaging technology concept suitable for space applications, based on the assembly of vertically stacked sub-modules made by hybrid circuit metal-ceramic LTCC package technology, was already validated in [14]–[16]. The TRM demonstrator proposed in [15] combines the well-established Low Temperature Cofired Ceramics (LTCC) technology for space applications [17], together to the assembly technique that is being developed in the past decades at package and chip level for various applications (i.e. avionic, commercial, etc. [18]–[22].

The main goal of the initial work presented in [15] was the significant reduction of the TRM footprint to allow for

the placement of a higher number of modules on a given patch antenna array panel area (and so enabling both a higher beam steering capability [23] and higher power density for improved antenna performance). However, this first demonstration vehicle left out several aspects in order to save module real-estate, to limit its design complexity, and to avoid that too many development objectives might invalidate the overall research project. As an example, the possibility to perform calibrations both at module and at antenna instrument level, which is a typical feature of T/R modules for space Synthetic Aperture Radar (SAR) applications [23]–[26], was left as a potential upgrade to be addressed in the frame of future development. The work of this paper went in the direction of filling such gap, as a first mandatory improvement for the use of the 3D interconnect technology and dice placement approach on real space products.

On the other hand, transfer of heat from the 3DTRM to the equipment at antenna level is of primary concern, and the means for conveying the heat from the external surface of the module to the satellite sink have to be carefully devised. To this aim, to allow the heat from the HPA MMIC reaching the external module surface toward the thermal extraction harness at equipment level with minimum impact on junction temperature, all the materials used for the construction of the 3DTRM that make up such thermal path have also to be engineered and optimized. As a side constrain, the module power added efficiency (PAE) comes also into play, and ways of increasing such key feature need to be devised.

Heat extraction capability from the active power components assembled in the 3DTRM imposes an upper boundary on the maximum saturated RF power that the module can deliver, given the constraint on the highest junction temperature (Tj) that the HPA MMIC can reach while still meeting the derating requirements applicable to space applications [27]. Such constrain is also determined by the HPA MMIC bulk semiconductor technology (GaAs or GaN).

The work presented in this paper gathers all the above mentioned aspects and translates them into a consolidated technology aiming at manufacturing and testing a set of second generation 3DTRM design demonstrators able to address the following main goals:

- Introduction of the module calibration feature,
- Extension of the GaN MMIC technology for to the HPA MMIC, in order to increase the maximum module output power and to improve the module PAE,
- Optimization of the heat extraction capability;
- Operating bandwidth of at least 2 GHz (X band), needed to increase the range resolution,
- Footprint reduction to allow a further increase of array beam forming agility and power density.

Planar SAR antennas based on arrays of radiating elements closely spaced to maximize beam forming agility [23] are the type of antennas that mostly benefit from a packaging approach aimed at minimizing module footprint, like the one described in this work. The long term, tight hermeticity requirement is mandatory for highly reliable space applications, and for this reason our development is focused on a packaging concept based on materials and processes that guarantee such compliance [15]–[27].

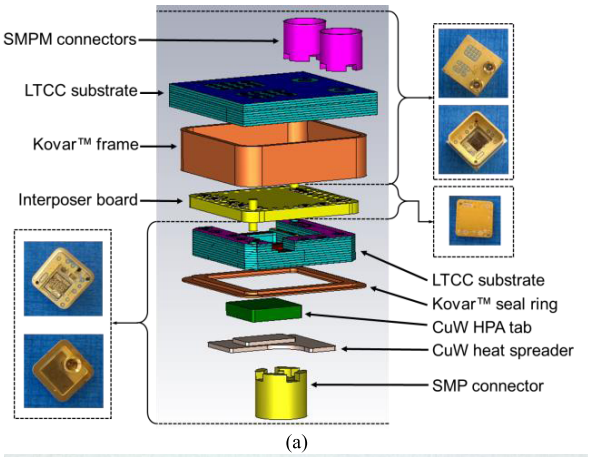

(a)

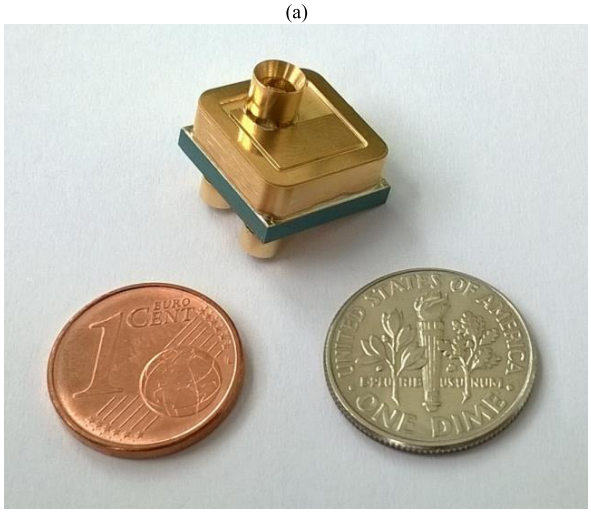

(b)

FIGURE 1. (a) Module constructional schematics: the top semi-module is the one that hosts the core-chip, while the lower semi-module contains the HPA, LNA and SPDT MMIC's. The interposer connector (board) is placed between the two modules, and is enclosed in the hermetic cavity following assembly and seam-sealing operation. (b) A picture of the fully assembled module is shown.

II. MODULE DESCRIPTION

By following the same constructional approach of the original development work [15] as shown in Fig. 1, the new 3DTRM package is made up of two semi-modules, each one being a hermetic metal ceramic housing itself. The back-end semi-module contains the metallic frame that makes up the internal hermetic cavity, and two Subminiature Modular Plugin Mini (SMPM) connectors (TX input and RX output) non-hermetically soldered to the LTCC substrate. The other semi-module (the front-end one) contains one Subminiature Modular Plugin (SMP) antenna connector and the lid; the latter being hermetically soldered to the ceramics. A copper-tungsten (CuW) heat-sink is also soldered to the front-end package hermetically closing the LTCC substrate, as can be seen in Fig. 1a.

A brief description of the multilayer LTCC substrate stack-up follows:

- LTCC system: GreenTape^{TM} 951 (ε_r = 7.8, loss tangent = 0.0140, both @ 10 GHz),
- number of layers: 10 for both the back-end and the front-end LTCC substrates,
- green tape thickness: 165.1 μm and 254.0 μm.

As a baseline constructive approach, the HPA MMIC is soldered with eutectic gold-tin (AuSn) alloy to a CuW tab, which in turn is attached to the package heat sink by means of a high thermal conductivity epoxy resin.

The last step in the assembly of the 3DTRM hybrid circuit consists in the seam welding of the front-end semi-module sealing ring to the frame of the back-end semi-module, both of which are made in Kovar®. In this way, a hermetic, thus suitable for space applications, ''full'' package is obtained. The overall height of the module is ∼6.1 mm (∼13 mm if connectors are included).

The above two semi-modules are electrically connected to each other by means of a passive interposer board shown in Fig. 1.

Two different versions of the 3DTRM were designed based on a different HPA GaN MMIC. The set of active components that were common to both versions was the following:

- an X-band LNA MMIC in pHEMT 0.15 μm GaAs technology: P/N TGA2512 from [29],
- a DC to 12 GHz High Power SPDT switch MMIC in 0.25 μm GaN technology: P/N TGA2352 from [29],
- a 6-bit X-Band TASI custom design core-chip MMIC in 0.18 μm Enhancement/Depletion (E/D) GaAs technology.

Version 1 (V1) of the 3DTRM demonstrator was designed using an X-Band HPA GaN MMIC P/N CHA8610-99F procured from [28], while version 2 (V2) was based on P/N TGA2624 from [29]. The reason for engineering two versions of the module was to demonstrate a wider bandwidth at a ''baseline'' transmission power capability with V1 parts, and a high power demonstrator, even if with a narrower useful bandwidth imposed by the MMIC itself, with V2 parts.

As a further improvement with respect to the initial concept in [15], which resulted in a rectangular footprint of about 13.4mm × 16.4mm, the proposed design was able to achieve a square 13.8 mm × 13.8 mm footprint, fully complying with the target set to be less than 14.0 mm × 14.0 mm.

III. ELECTRICAL DESIGN

In order to get closer to a demonstrator of a T/R module design suitable for space SAR antenna applications, the main needed circuitry implementation was the capability to perform an accurate SAR antenna calibration without any increase in module footprint. High calibration accuracy implies good isolation between the calibration paths, to minimize disturbances and thus to optimize the accuracy of amplitude and phase of the transmitting and receiving signals [30], [31]. The sampling of the RF signal at the antenna port for calibration is typically achieved with the implementation of a planar coupled-line directional coupler. A parallel coupled line microstrip based coupler can be employed; however, this approach allows only limited values of isolation and directivity as long as no compensation techniques for equalizing even and odd mode phase velocities are used [32], [33]. This work targeted a challenging 40 dB isolation for the coupling structure based on a coupling factor of 27 dB with at least 2 GHz bandwidth. The block diagram of the re-designed 3DTRM is shown in Fig. 2.

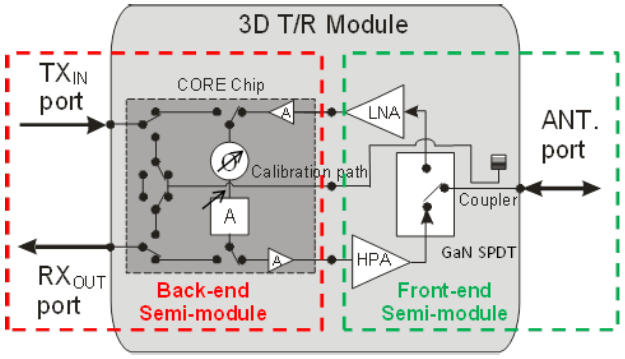

FIGURE 2. Re-designed 3DTRM block diagram.

Some real estate on the front-end module footprint needed to be sacrificed for the purpose of integrating the directional coupler, which led to further push the technology going beyond the current LTCC layout design rules, e.g., screen printed line width and gap, distance of track from substrate edge, maximum number of stacked vias, among others. In Fig. 3 the area devoted to the coupler integration is shown.

The strict constrains in terms of isolation and directivity values, as well as on the limited layout area, suggested to implement the directional coupler in a mixed 3D stripline/coplanar configuration. Part of the layout of the implemented coupler can be seen also in Fig. 3.

The module area available for the coupler was quite limited, and did not allow to follow the usual λ/4 coupler design. So, the coupled portion in Fig. 3 was implemented as a curved combined stripline-coplanar transmission line. Impedance discontinuities occur at both ends of the stripline-coplanar section; a stripline to microstrip transition exists toward the SPDT and toward the resistive termination, and a stripline to coaxial transmission line transition occurs at the antenna SMP connector side.

Therefore, although the first draft design of the coupler was initially carried out following the theory reported in [34] by appropriately setting the even and odd impedances associated to the coupled section, the final design was achieved through a set of full-wave simulations. In particular, one of such optimization steps allowed finding the appropriate values of the distance between the two lines to achieve the desired values of directivity and isolation.

All the EM simulation work was carried out using the CST Microwave Studio 2016 environment [35].

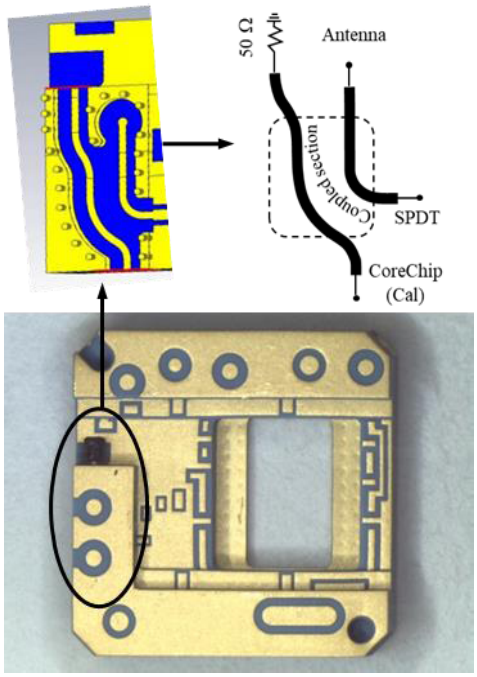

FIGURE 3. Front-end semi-module LTCC substrate showing (dark ellipsis) the area devoted to the directional coupler integration inside the LTCC multilayer: an enlarged detail of the stripline-coplanar structure inside the circled area is also shown. The coupler area is 2.1 mm × 1.4 mm, the coupled lines are 150 μm wide, the gap between coupled lines is 534 μm and the line to ground spacing is 276 μm. The through cavity hosts the mesa of the heatsink (see Fig. 6).

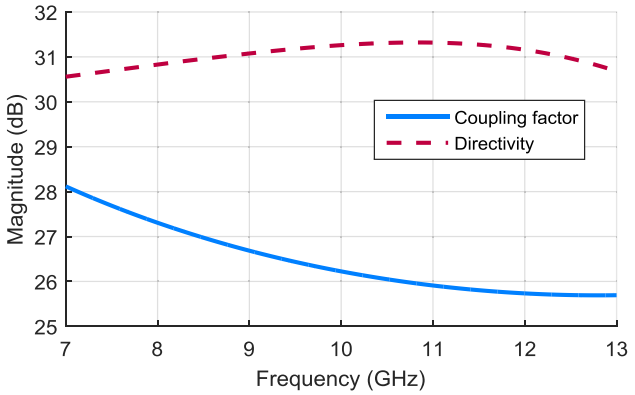

FIGURE 4. Simulated coupling factor and RX directivity (port isolation in RX mode); design target values were 27 ± 1 dB and >25 dB in the full Xband, respectively.

Fig. 4 shows the simulated performance of the circuit section that includes the directional coupler, and that embraces the path from the calibration terminal on the front-end semi-module to the antenna port (SMP connector). This specific simulation task was carried out in a dedicated simplified model, in order to fine tune the most critical sections of the various involved transmission line paths, i.e. from the coupler toward the core-chip pad on the back-end sub-module. The coupling factor target specification was 27 dB, whereas a value higher than 25 dB for the directivity in RX calibration mode was required.

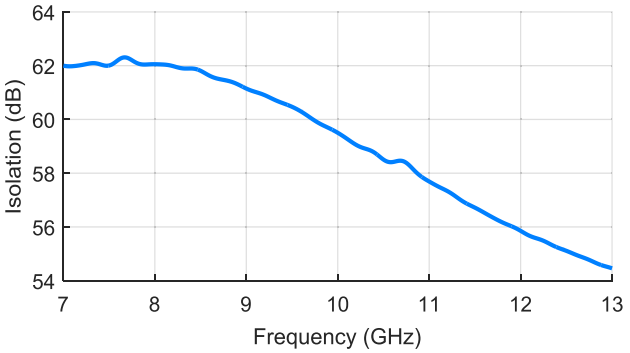

FIGURE 5. Simulated isolation between the antenna port and the calibration input pad at the core-chip.

Fig. 5 shows the EM simulated plot of the isolation between the antenna port and the calibration input pad at the core-chip. This parameter is of very high concern when calibrating the antenna instrument: the path from the core-chip calibration port, through the coupler and then along the RX path back to the core-chip (see Fig. 11-a), has to be isolated as much as possible from the antenna port. This avoids spurious coupling of the calibration signal to nearby T/R modules, leading to a lower SAR antenna instrument calibration effectiveness. This is one of the main reasons why a high directivity value for the directional coupler is so important.

The EM simulation does not take into account the electrical parameters of the active components (the terminating ports at the SPDT switch pad and at the core-chip calibration pad); these two relevant ports are terminated by an ideal 50 Ω load; this simplification was expected to lead to worst measured isolation values on the real T/R module prototypes.

IV. PACKAGE THERMAL DESIGN IMPROVEMENT

Package thermal design is of key importance for space applications in which high power signals are to be dealt with, as in our case, since maximization of the output power and the PAE in TX mode are a key system requirement [36]. In particular, a PAE of at least 30% for both module versions was given as a target for the new demonstrator. In order to improve the heat extraction capability of the package with respect to the package-heatsink assembly in [15], the front-end semi-module LTCC substrate has been redesigned with a through-cavity, as shown in Fig. 3. This cavity now allows for the placement of a hermetically soldered heatsink in direct contact with the heat-spreading tab to which the HPA MMIC is AuSn soldered. Basically, the heatsink is shaped to have a smaller protrusion (the mesa) that reaches directly the HPA tab, as shown in Fig. 6. The CuW tab is attached to the heatsink by means of a high thermal conductivity epoxy resin, as a baseline approach.

This innovative solution overcomes the "thermal barrier" present in [15] by having the ceramic material between the HPA heat-spreading tab and the external heatsink completely removed. The total thermal resistance seen by the backside of

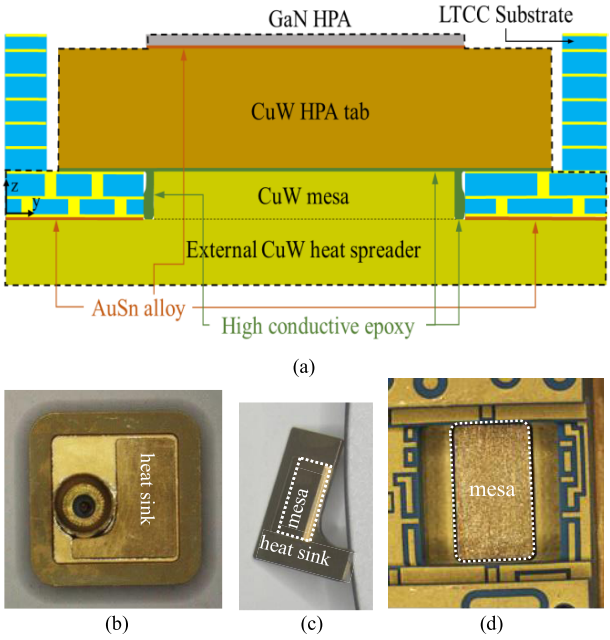

FIGURE 6. View of the hermetically soldered copper-tungsten heatsink-mesa: a) cross-sectional view, b) external module view after soldering the heatsink to the LTCC substrate, c) before soldering, and d) the internal view of the module: the mesa inset can be seen within the LTCC through-cavity shown in Fig. 2. The mesa dimensions are 2.94 mm × 5.26 mm × 0.43 mm.

the HPA MMIC toward the external surface of the sink (from which the heat is extracted at system level) is so drastically reduced.

As a consequence, the increase of the HPA junction temperature with respect to the external satellite thermal radiator temperature will be quite limited.

The above strategy constitutes a ''first step'' of improvement. Another important contribution to the reduction of the thermal resistance from the HPA MMIC junction to the external thermal interface comes from the use of a higher thermal conductivity material to be used for the HPA tab. Although much more expensive, the copper-diamond (Cu-D) composite has roughly twice the thermal conductivity of CuW, which means a non-negligible increase in the heat extraction capability of the package.

Finally, for a furtherly enhanced package configuration, the last contribution to the heat drain capability improvement consists in the use of AuSn alloy also for the attachment of the tab, instead of using an epoxy resin. However, the successful and reliable implementation of this additional thermal improvement, thus without impacting the module's capability for long-term hermeticity, requires that the attachment of the seal ring and the heatsink/mesa insert into the LTCC substrate have to be carried out using a higher melting point alloy, like gold-germanium (AuGe), to avoid reflowing the alloy in the hermetic junctions during the AuSn soldering of the tab.

The validity of the above mentioned assembly strategies is confirmed by thermal simulations run using MSC NASTRAN [37]. The objective is to compare the improvement in terms of heat draining capability that can be obtained with the enhanced configuration (Cu-D tab attached with AuSn alloy) with respect to the baseline one (CuW tab attached with epoxy resin). Moreover, the obtained results are also compared to those reported in [15] where the preliminary 3D package demonstrator had a limited heat extraction capability due to the LTCC barrier between the HPA tab and the heatsink.

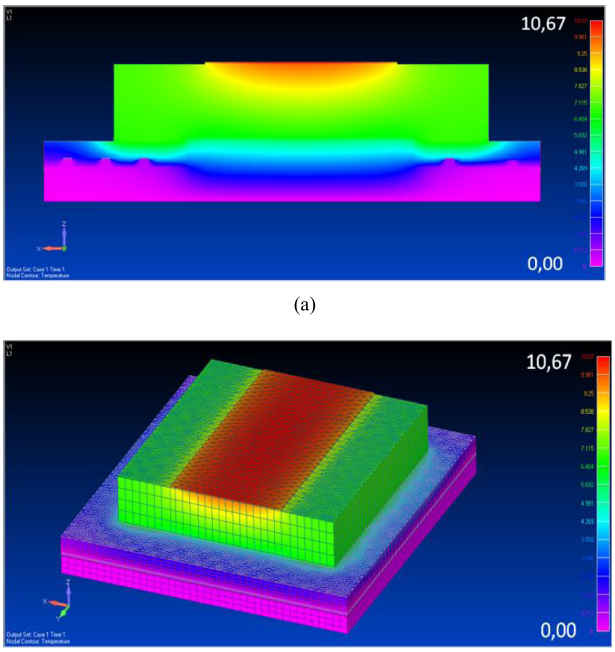

FIGURE 7. Thermal simulation showing the temperature distribution in the enhanced configuration of the package: a Cu-D tab soldered with AuSn to the CuW heat sink. (a) Cross-sectional view, (b) full 3D view.

Fig. 7 shows the temperature distribution in the enhanced case. A similar pattern is obtained in the baseline case; however, the gain in terms of temperature reduction is in the order of 33 % having 10.67 °C of temperature increase for the enhanced configuration to be compared to the 15.37 °C of the baseline one. The initial value achieved in [15] was 29.26 °C. Thermal boundary conditions were set to adiabatic, and a conduction heat transfer only towards the heat spreader in contact with an infinite sink at 0 °C was assumed. In addition, the heat at the backside of the HPA MMIC was assumed to be evenly distributed, with thermal power set at 22.5 W.

V. ELECTRICAL CHARACTERIZATION OF A PROTOTYPE RUN

A. TEST BENCH SET-UP AND GENERAL RF PERFORMANCE

Fig. 8 shows the measurement set-up. Commands to the core-chip of the 3DTRM are sent using a custom-built text fixture (''black box'' shown in the figure close to the holder interface). A Rohde&Schwarz model ZVT 20 Vector Network Analyzer (VNA) was used, together with a pulse generator, 3 power supplies, and an oscilloscope. Power supply pulse

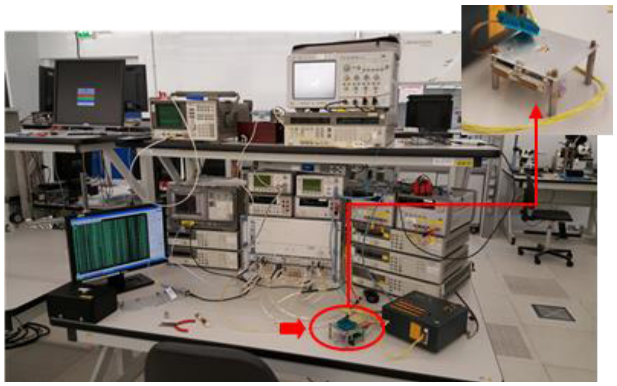

FIGURE 8. Measurement set-up: the holder interface in which the 3DTRM is placed for testing has been red-circled and zoomed.

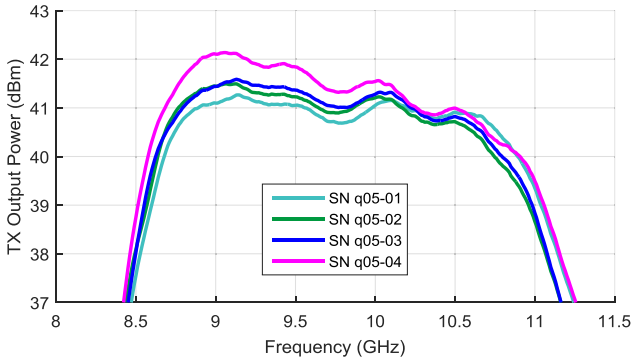

FIGURE 9. Measured TX parameters at 5 dB compression point on 4 prototypes of V2 version.

generation circuitry (not shown) was assembled on the back side of the holder interface.

Due to the insufficient gain at core-chip level, it was not possible to drive the version V1 of the 3DTRM in full compression mode, making a measurement of the useful bandwidth on those devices not of interest for the scope of the present work. Apart from the useful bandwidth, all the most important parameters characterizing T/R modules were successfully measured on parts from both versions.

TABLE 1. Main measured electrical parameters.

3DTRM version	V1	V2
Maximum linear TX gain (dB)	43.1	51.5
Linear RX gain (dB) @ f = 9.5 GHz	41	
1dB bandwidth (GHz) @ 5 dB compression point (max PAE from [30]), 10% DC	N.A.	2.1
1dB bandwidth (GHz) @ 10 dB compression point, 10% DC	N.A.	2.3
Peak TX output power (dBm) @ 9.5 GHz, 10% DC	39.2	41.4/41.8*
Noise figure (dB), minimum	3.26	
Effective average coupling factor (dB)	28.0	
Minimum isolation in RX calibration mode (dB)	40.5	42.1

* Enhanced version q05-04

Table I shows a summary of the main electrical parameter measurements made on a prototype lot of 7 parts in total: 3 modules of version V1 and 4 modules of version V2. One sample of the V2 group was built in the enhanced package configuration described in Section IV, and was identified with the serial number (S/N) q05-04.

Fig 9 shows the TX output power at 5 dB compression point (CP) measured on the 4 prototypes of version V2. This CP value was chosen to obtain the maximum PAE as per relevant curves in the HPA V2 datasheet. As expected, the enhanced version S/N q05-04 (purple curve) performed better than the other (baseline) parts.

Obviously, the measurement made on a single prototype, due to the limited availability and costs of the Cu-D tab, cannot be fully significant, i.e. the specific HPA could be by chance performing better than the others; thus, the limited increase of the output power (≈0.4dB) may not be due to the more effective heat extraction; nevertheless, the SN q05-04 results still demonstrate the reliable assembly and use of the HPA mounted on the Cu-D tab.

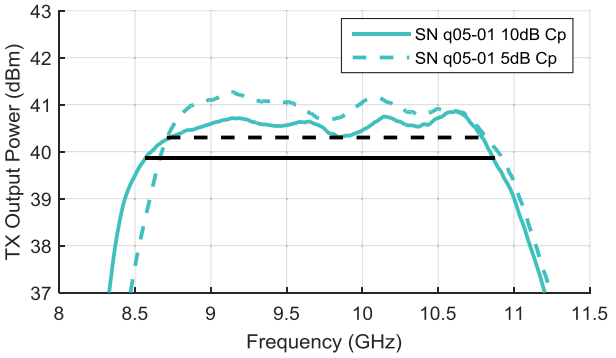

FIGURE 10. TX Power Output for two different compression point measurements on prototype q05-01 (V2 version). The black lines show the bandwidth at 1 dB gain flatness.

Fig 10 shows the TX Power Output for two different CP measurements on prototype q05-01 (V2 version). By increasing the CP, a 10% bandwidth increase (from 2.1 GHz to 2.3 GHz) was achieved; this obviously led to a worsening of the PAE (from 31.2 % to 28.9 %).

Finally, the measured values of PAE at module level for different settings of the Pulse Repetition Frequency (PRF), duty cycle (DC) and pulse width were all higher than 30 %. PAE measurements were performed at 5 dB CP in continuous wave (CW) mode at 9.5 GHz, by taking into account both control and RF circuitry power consumption values.

B. MODULE CALIBRATION FEATURE VALIDATION

A brief description of the measurement procedure followed to obtain the equivalent coupling and isolation values follows. Please refer to Fig. 11.

First of all, the following measurement quantities are defined:

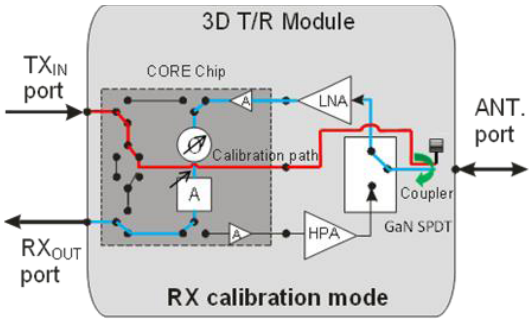

(a)

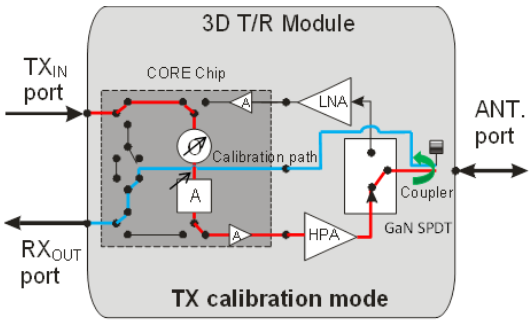

(b)

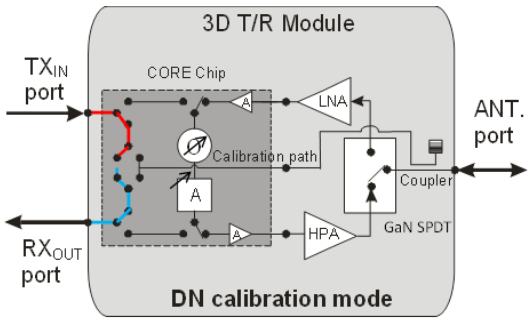

(c)

FIGURE 11. 3DTRM calibration modes: forward calibration signal path shown in red, return path in blue. Green arrow represents signal coupling across the embedded directional coupler.

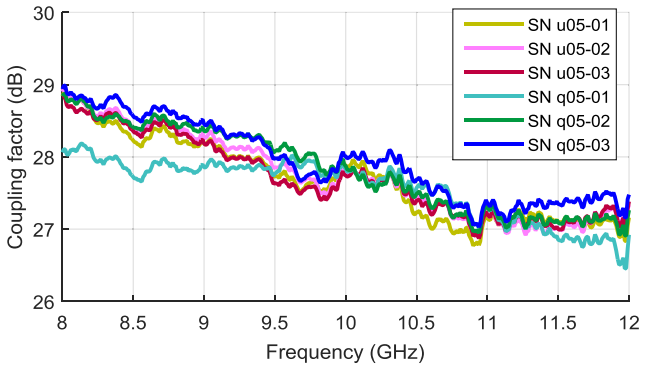

FIGURE 12. Equivalent coupling factor measured on 6 prototypes.

- *TX*– gain in nominal TX mode,
- *RX*– gain in nominal RX mode,
- RX_{CAL} – gain in RX calibration mode (Fig. 11-a),

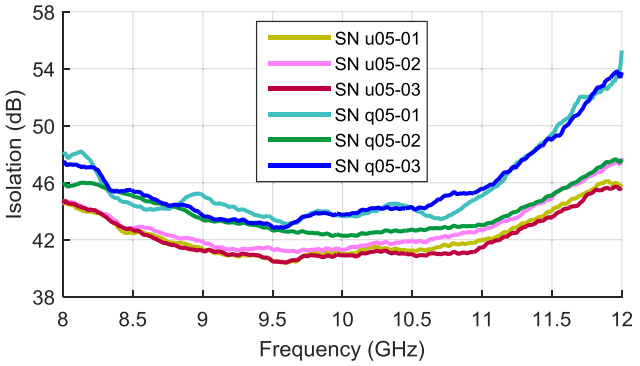

FIGURE 13. Measured antenna port isolation in RX calibration mode (6 prototype parts were measured).

- TX_{CAL} – gain in TX calibration mode (Fig. 11-b),
- DN_{CAL}– loss of the "short calibration" path between the RX$_{OUT}$ port and the TX$_{IN}$ ports (Fig. 11-c).

For the evaluation of the "effective" coupling factor (ECF), defined as the directional coupler coupling coefficient plus losses in the calibration path, the simple calculation in (1) is performed:

$$\mathrm{ECF} = ((TX_{CAL} - TX) + (RX_{CAL} - RX) - DN_{CAL})/2 \tag{1}$$

All 3DTRMs were driven at 5 dB CP during both *TX* and TX_{CAL} measurements, whereas they were operated in their linear region during *RX* and RX_{CAL} measurements. In order to ensure that the RX amplifier chain operated under the same (linear) conditions during both *RX* and RX_{CAL} measurements, when measuring RX_{CAL} a suitable input power level at the TX$_{IN}$ port was applied to obtain roughly a −30 dBm coupled signal level at the beginning of the return path. The same input power level of −30 dBm was also applied at the antenna port during the *RX* test.

As already explained in Section III, the isolation measurements, plotted in Fig. 11, are carried out in RX calibration mode in order to assess the leakage at the antenna port that will affect the instrument calibration in real operational conditions [31].

Fig. 12 shows the obtained ECF, as measured from the antenna port to the calibration output port (which is the RX$_{OUT}$ port connector in our case), on 6 parts built in the standard package configuration. Very low dispersion around the 28 dB average value can be seen.

Fig. 13 shows the measured isolation values between the antenna port and TX$_{IN}$ port in RX calibration mode. The measurement is taken on the antenna port in RX calibration mode, so that it represents the leakage of the calibration signal that is injected through the TX$_{IN}$ port into the calibration path (see Fig. 11-a) and reaches the antenna port through the directional coupler isolated port. It can be seen that the lowest value is higher than 40 dB: the observed discrepancy from simulation results (see Fig. 5) is mainly due to the

TABLE 2. Comparison between the proposed high power 3D T/R module and other reported works.

	NF (dB)	RX gain (dB)	TX linear gain (dB)	Output power (W)	Footprint (mm x mm)	Internal calibration	Designed for Space
Proposed	**3.26 (min)**	**41**	**51.5 (max)**	**15 (41.8 dBm, max)**	**13.8 x 13.8**	**Yes**	**Yes**
Ref [15]	3.1-3.5	42-38	50 (max)	5-6 (37-38 dBm)	13.4 x 16.4	No	Yes
Ref [20]	3-4.5	27-25	N.A.	5-6[1]	~30x30	N.A.	No
Ref [18], Table II	6.3-7.8	19.5	41.25 (max)	5-9.5 (37-40 dBm)	20x20	No	No
Ref [17]	2.7-2.8	30.5-29	N.A.	2 (33 dBm)	20x20	No	No

[1] No data/figure available, only a statement saying that "Five to 6 W of transmit power were also demonstrated from 7.5-10 GHz".

mismatch of MMIC's that is not taken into account in full wave simulations.

In Table 2, the electrical performances and other key features of the proposed module are compared with those of other reported works. It seems quite clear that the proposed module reaches very good overall performances by combining good RX characteristics in terms of gain and noise figure, together with very large TX gain and output power.

VI. CONCLUSION

As a result of further R&D work on our original concept, a high performance evolution of the advanced 3DTRM was successfully demonstrated. In addition to implementing the innovative stacking technology for space applications, and thus using 3D interconnection techniques, such module was upgraded by integrating the calibration feature, improving the heat extraction capability and extending the use of GaN MMIC technology to the power section of the module.

Two different versions of the 3DTRM were designed and tested, each based on a different HPA MMIC (see Section II).

The version V1 allowed us to demonstrate a wider bandwidth at a "baseline" transmission power capability, whereas the version V2 was engineered as a high power demonstrator, even if with a narrower useful bandwidth imposed by the MMIC itself.

Successful demonstration of:

- calibration feature performance in terms of excellent antenna port isolation in RX calibration mode (better than 40 dB), and low variability of coupling factor among different modules,
- high compressed TX power output,
- high efficient heat extraction
- wide useful bandwidth, and
- square footprint

confirms that the evolution of the original 3D hermetic packaging and interconnect integration concept is directly applicable to high performance SAR antennas for space applications.

On the basis of the work described in this paper, a patent application was filled [16].

ACKNOWLEDGMENT

The authors would like to thank Massimo Molinari from TASI for his valuable support to the RF testing set-up implementation and during the testing campaign, Ernesto Di Paola from TASI for his contribution to the LTCC engineering, manufacturing processes fine tuning and thermal evaluation activities, and Elio Picchione from TASI who was in charge of the set-up of the MMIC and package soldering processes.

REFERENCES

[1] H. Matevosyan, I. Lluch, A. Poghosyan, and A. Golkar, "A value-chain analysis for the copernicus earth observation infrastructure evolution: A knowledgebase of users, needs, services, and products," *IEEE Geosci. Remote Sens. Mag.*, vol. 5, no. 3, pp. 19–35, Sep. 2017.

[2] E. Alarcón *et al.*, "Design and optimization of a polar satellite mission to complement the copernicus system," *IEEE Access*, vol. 6, pp. 34777–34789, 2018.

[3] J. Ma, W. Sun, G. Yang, and D. Zhang, "Hydrological analysis using satellite remote sensing big data and CREST model," *IEEE Access*, vol. 6, pp. 9006–9016, 2018.

[4] X. Bian, Y. Shao, S. Wang, W. Tian, X. Wang, and C. Zhang, "Shallow water depth retrieval from multitemporal sentinel-1 SAR data," *IEEE J. Sel. Topics Appl. Earth Observ. Remote Sens.*, vol. 11, no. 9, pp. 2991–3000, Sep. 2018.

[5] H. Joerg, M. Pardini, I. Hajnsek, and K. P. Papathanassiou, "Sensitivity of SAR tomography to the phenological cycle of agricultural crops at X-, C-, and L-band," *IEEE J. Sel. Topics Appl. Earth Observ. Remote Sens.*, vol. 11, no. 9, pp. 3014–3029, Sep. 2018.

[6] B. T. Le *et al.*, "Coal exploration based on a multilayer extreme learning machine and satellite images," *IEEE Access*, vol. 6, pp. 44328–44339, 2018.

[7] W. Xu, Y. Deng, and R. Wang, "Multichannel synthetic aperture radar systems with a planar antenna for future spaceborne microwave remote sensing," *IEEE Aerosp. Electron. Syst. Mag.*, vol. 27, no. 12, pp. 26–30, Dec. 2012.

[8] A. Golkar and I. Lluch i Cruz, "The federated satellite systems paradigm: Concept and business case evaluation," *Acta Astron.*, vol. 111, pp. 230–248, Jun. 2015.

[9] M. Lörcher and H. Brugger, "Advanced RF sensors for SAR earth observation using high precision T/R-Modules," in *Proc. 3rd Int. Asia-Pacific Conf. Synth. Aperture Radar (APSAR)*, Seoul, South Korea, Sep. 2011, pp. 1–6.

[10] C. Andricos, S. Yueh, V. A. Krimskiy, and Y. Rahmat-Samii, "Compact KU-band T/R module for wide-swath high-resolution radar imaging of cold land processes," NASA Tech Briefs, Tech. Rep. NPO-46428, Mar. 2010, pp. 27–28. [Online]. Available: https://ntrs.nasa.gov/search.jsp?R=20100009683

[11] P. Schuh *et al.*, "T/R-module technologies today and possible evolutions," in *Proc. Int. Radar Conf. 'Surveill. Safer World' (RADAR)*, Bordeaux, France, Oct. 2009, pp. 1–5.

[12] Y. Mancuso and C. Renard, "New developments and trends for active antennas and TR modules," in *Proc. Int. Radar Conf.*, Oct. 2014, pp. 1–3.

[13] N. J. Kolias and M. T. Borkowski, "The development of T/R modules for radar applications," in *IEEE MTT-S Int. Microw. Symp. Dig.*, Montreal, QC, Canada, Jun. 2012, pp. 1–3.

[14] A. Fina *et al.*, "An advanced transmit/receive 3D ceramic hybrid circuit module for space applications," in *Proc. Eur. Microw. Conf. (EuMC)*, Paris, France, Sep. 2015, pp. 785–788.

[15] A. Di Carlofelice, F. de Paulis, A. Fina, U. Di Marcantonio, A. Orlandi, and P. Tognolatti, "Compact and reliable T/R module prototype for advanced space active electronically steerable antenna in 3-D LTCC technology," *IEEE Trans. Microw. Theory Techn.*, vol. 66, no. 6, pp. 2746–2756, Jun. 2018.

[16] A. Fina *et al.*, "Microwave antenna module for space applications including a hybrid transmit/receive module of package on package type," Italian Patent Office, Application Number IT102017000086529, EU Patent 18 186 105.5, U.S. Patent 16/047.407, Jul. 27, 2017.

[17] Z. J. Yu, Z. Xu, Y.-K. Deng, and Z.-G. Zhang, "An overall LTCC package solution for X-band tile T/R module," *Prog. Electromagn. Res. Lett.*, vol. 38, pp. 181–192, 2013. [Online]. Available: http://www.jpier.org/PIERL/pier.php?paper=13011009
[18] S.-K. Yeo, J.-H. Chun, and Y.-S. Kwon, "A 3-D X-band T/R module package with an anodized aluminum multilayer substrate for phased array radar applications," *IEEE Trans. Adv Packag.*, vol. 33, no. 4, pp. 883–891, Nov. 2010.
[19] B. Bonnet *et al.*, "3D packaging technology for integrated antenna front-ends," in *Proc. 38th Eur. Microw. Conf.*, Oct. 2008, pp. 1569–1572.
[20] M. S. Hauhe and J. J. Wooldridge, "High density packaging of X-band active array modules," *IEEE Trans. Compon., Packag. Manuf. Technol. B*, vol. 20, no. 3, pp. 279–291, Aug. 1997.
[21] J. Cho *et al.*, "Si-interposer design for GPU-memory integration concerning the signal integrity," in *Proc. DesignCon*, Santa Clara, CA, USA, Jan. 2013.
[22] M. Swaminathan, "Electrical design and modeling challenges for 3D system integration," in *Proc. DesignCon*, Santa Clara, CA, USA, Jan. 2012.
[23] R. J. Mailloux, "Phased array theory and technology," *Proc. IEEE*, vol. 70, no. 3, pp. 246–291, Mar. 1982.
[24] A. Klaassen, R. Reber, and M. Ludwig, "A precision T/R module for X-band SAR applications with a transmit chain in HBT-technology," in *Proc. Gallium Arsenide Appl. Symp. (GAAS)*, Bologna, Italy, Oct. 1999, pp. 4–5.
[25] B. Braeutigam, J. H. Gonzalez, M. Schwerdt, and M. Bachmann, "Radar instrument calibration of TerraSAR-X," in *Proc. 7th Eur. Conf. Synth. Aperture Radar (EUSAR)*, Jun. 2008, pp. 1–4.
[26] R. Torres and M. Zink, "Efficient calibration of active phased-array SARs," in *Proc. Eur. Conf. Synth. Aperture Radar (EUSAR)*, 2006.
[27] *Space Product Assurance–Derating–EEE Components*, document ECSS-Q-ST-30-11C Rev 1, ESA-ESTEC, Oct. 2011.
[28] [Online]. Available: https://www.ums-gaas.com/
[29] [Online]. Available: https://www.qorvo.com/
[30] S. J. Horst *et al.*, "Implementation of RF circuitry for real-time digital beam-forming SAR calibration schemes," in *Proc. IET Int. Conf. Radar Syst.*, Oct. 2012, pp. 1–6, doi: 10.1049/cp.2012.1603.
[31] B. Brautigam, M. Schwerdt, M. Bachmann, and M. Stangl, "Individual T/R module characterisation of the TerraSAR-X active phased array antenna by calibration pulse sequences with orthogonal codes," in *Proc. IEEE Int. Geosci. Remote Sens. Symp.*, Barcelona, Spain, Jul. 2007, pp. 5202–5205.
[32] S. Maheswari and T. Jayanthy, "High directivity microstrip coupler using variable width structure," *IOSR J. Electron. Commun. Eng.*, vol. 9, no. 4, pp. 24–28, Jul./Aug. 2014.
[33] M. Moradian and M. Khalaj-Amirhosseini, "Improvement the characteristics of the microstrip parallel coupled line coupler by means of grooved substrate," *Prog. Electromagn. Res. M*, vol. 3, pp. 205–215, 2008. [Online]. Available: http://www.jpier.org/PIERM/pier.php?paper=08071205
[34] D. M. Pozar, *Microwave Engineering*, 3rd ed. Hoboken, NJ, USA: Wiley, 2005.
[35] Computer Simulation Technology, CST Studio. (2016). [Online]. Available: https://www.cst.com/products/csts2
[36] L. D. Castillo, T. Thrivikraman, J. P. Hoffman, J. Miller, G. Birur, and T. R. Knowles, "Robust, reworkable thermal electronic packaging: Applications in high power TR modules for space," in *Proc. IEEE Aerosp. Conf.*, Mar. 2013, pp. 1–10.
[37] *MSC NASTRAN*. Accessed: Sep. 2018. [Online]. Available: http://www.mscsoftware.com/it/product/msc-nastran

ANTONIO FINA received the Laurea degree in electronics engineering from the University of L'Aquila, L'Aquila, Italy, in 1991.

He joined Thales Alenia Space, L'Aquila, as a Tests and Qualifications Engineer, where he was focused on hybrid circuits for space applications, and was then the Head of the Microelectronics Technology Unit from 1998 to 2011, and later a Technology and Technical Officer from 2011 to 2014. He is currently the Head of the Microelectronics Research and Development Unit, a Thales Alenia Space Expert in microelectronics technology, exercising the role of Design Authority for product line, technology, T/R modules, and SAR electronic front end assemblies since 2017.

ALESSANDRO DI CARLOFELICE received the Laurea degree in electronic engineering from the University of L'Aquila, L'Aquila, Italy, in 2006, and received the Ph.D. degree in microwave radiometry for remote sensing and bio-medical applications in 2011.

Since 2011, he has been with the Department of Electrical Engineering and Information, University of L'Aquila, as a Post-Doctorate Researcher. His research activity is in the field of space systems for telecommunications and remote sensing.

FRANCESCO DE PAULIS (S'08–M'13) was born in L'Aquila, Italy, in 1981. He received the Specialist degree (*summa cum laude*) in electronic engineering from the University of L'Aquila, L'Aquila, in 2006, the M.S. degree in electrical engineering in 2008, and the Ph.D. degree in electrical and information engineering from the University of L'Aquila, in 2012. In 2006, he joined the EMC Laboratory, Missouri University of Science and Technology (formerly the University of Missouri-Rolla), USA.

He was involved in the research activities at the UAq EMC Laboratory from 2004 to 2006, L'Aquila, and at the MST EMC Laboratory from 2006 to 2008, Rolla MO, USA. From 2004 to 2005, he had an internship at Selex Communications, L'Aquila (now Leonardo s.p.a.), within the layout/SI/PI design group. He is currently a Researcher at the UAq EMC Laboratory, University of L'Aquila, Italy. His main research interests are in SI/PI design on PCB, packages interposers and chips, analysis and characterization of composite materials for shielding, RF interference in mixed-signal system, TSVs in silicon chips and interposers, EMI problem investigation, EMC measurements based on NF-FF transformation techniques, remote fault detection in transmission lines, design of T/R modules, and electronic systems for space applications.

He received the Past President's Memorial Award in 2010 from the IEEE EMC Society. He was a recipient of the Best Paper Award in 2010, 2013, and 2016, respectively, and the Best Student Paper Award in 2009 and in 2011 at the IEEE International Symposium on EMC. He received the Paper Award in the power and RF design category in 2010, 2011, and 2012, respectively, at the IEC DesignCon. He was selected as the Distinguished Reviewer of the TRANSACTIONS ON EMC in 2014. He received the Honorable Mention for the Best Paper Award of the TRANSACTIONS ON EMC in 2014. He serves as an Associate Editor for the IEEE TRANSACTIONS ON EMC Letter.